Functional and Mechanistic Studies of Cytochrome c_3 from *Desulfovibrio gigas*: Thermodynamics of a "Proton Thruster" †

Ricardo O. Louro,‡ Teresa Catarino,‡ David L. Turner,‖,‡ M. Antonieta Piçarra-Pereira,‡ Isabel Pacheco,‡ Jean LeGall,§,‡ and António V. Xavier*,‡

Instituto de Tecnologia Química e Biológica−Universidade Nova de Lisboa, Rua da Quinta Grande, 6, Apt. 127. 2780 Oeiras, Portugal, Department of Biochemistry and Molecular Biology, University of Georgia, Athens, Georgia 30602, and Department of Chemistry, University of Southampton, Southampton SO17 1BJ, U.K.

Received June 25, 1998; Revised Manuscript Received August 17, 1998

ABSTRACT: Nuclear magnetic resonance and visible spectroscopies were used to determine the thermodynamic parameters of the four hemes in cytochrome c_3 from *Desulfovibrio gigas* at 298 and 277 K and to investigate the mechanism of electron/proton energy transduction. Data obtained in the pH range from 5 to 9 were analyzed according to a model in which the hemes interact with each other (redox cooperativities) and with an ionizable center (redox−Bohr cooperativities). The results obtained at the two temperatures allow the deconvolution of the entropic contribution to the free energy of the four hemes, to the acid−base equilibrium of the ionizable center, and to the network of cooperativities among the five centers. The redox potentials of the hemes are modulated by the enthalpic contribution to the free energy, and evidence for the participation of the propionates of heme I in the redox−Bohr effect is presented. The network of interactions between the centers in this protein facilitates the concerted transfer of electrons and protons, in agreement with the "proton thruster" mechanism proposed for electronic to protonic energy transduction by cytochromes c_3.

Tetraheme cytochrome c_3 is a periplasmic protein of sulfate-reducing bacteria, which couples the transfer of electrons and protons from hydrogenase (*1*, *2*) to the electron-transfer chain of sulfate respiration and to ATP synthase, respectively. It is a small (13.5−15 kDa) soluble protein containing four *c*-type hemes with each iron axially coordinated by two histidines and with different redox potentials. The available 3D structures (*3*−*8*) show that the architecture of the heme core is conserved, despite the low amino acid sequence homology, suggesting that this spatial organization is essential for the function of the protein.

The small size, stability, and high solubility facilitate the characterization of these proteins by a wide variety of techniques, including NMR[1] spectroscopy, which has been successfully applied in structural (*8*−*11*) and thermodynamic studies (*12*−*15*). It is possible to obtain unambiguous NMR assignments for the nuclei of the substituents of each heme in the structure (*16*−*19*) and to follow these signals through the different redox stages to determine their order of oxidation (*18*−*20*).

Redox titrations followed by NMR at various pH values allowed the determination of the microscopic thermodynamic properties of the *Desulfovibrio vulgaris* cytochrome c_3 (Dvc3) (*15*, *21*) within the framework of a model which considers five charged and interacting centers (four hemes and one ionizable center). This simple model has the advantage of requiring a relatively small number of parameters: four redox potentials, one pK_a, and six electron−electron (redox) and four electron−proton (redox−Bohr) interactions. From these studies and from potentiometric titrations of the oxidized and reduced forms, it was concluded that Dvc3 works as a "proton thruster" via a concerted two-electron/two-proton step in the physiological pH range (*22*), a functional complexity usually associated only with large energy-transducing transmembrane respiratory proteins. This step was shown to be crucial to maintain a high activity of hydrogen uptake by the periplasmic hydrogenase (*2*), which is fundamental for energy transduction in *Desulfovibrio* spp. (*2*, *23*).

Despite the considerable knowledge obtained for cytochrome c_3, a detailed molecular basis for its function is still lacking. This information may be obtained from studies in mutant proteins *(24)*, but comparison of naturally occurring varieties of cytochrome c_3 with different thermodynamic and structural properties may be more informative.

A previous study has provided a preliminary thermodynamic description of the cytochrome (*12*, *25*), but since then a new model has been developed which allows the redox and the redox−Bohr cooperativities to be deconvoluted. An extended thermodynamic description of Dgc3 is obtained in this work from studies made at two temperatures. A

† PRAXIS XXI Programme (BD 1509/93), EC grant CHRX-CT-940540, ERBFMRX-CT-98-0218.

* Phone: 351-1-4469820. Fax: 351-1-4428766. E-mail: xavier@itqb.unl.pt.

‡ Universidade Nova de Lisboa.

§ University of Georgia.

‖ University of Southampton.

[1] Abbreviations: Dgc3, Cytochrome c_3 from *Desulfovibrio gigas*; Dvc3, cytochrome c_3 from *Desulfovibrio vulgaris* (Hildenborough); SHE, standard hydrogen electrode; NMR, nuclear magnetic resonance; TRIS, tris(hydroxymethyl)aminomethane; NOE, nuclear Overhauser effect; NOESY, two-dimensional nuclear Overhauser enhancement spectroscopy.

10.1021/bi981505t CCC: $15.00
Published on Web 10/17/1998

comparison between Dgc3 and Dvc3 is then made, in an attempt to identify the physiologically meaningful characteristics of these proteins.

METHODS

Purification. *Desulfovibrio gigas* was grown as previously described, and the purification procedure was adapted from the literature (*26*). All buffers were prepared at pH 7.6. The cells were suspended in 0.01 M TRIS buffer with DNAse I and broken in a French press. The steps following were all performed at 4−6 °C. The cell paste was centrifuged for one and a half hours at 14 300 g to remove cell debris. The soluble fraction was centrifuged for 2 h at 150 000g, loaded onto a DEAE52 column equilibrated with 0.01 M TRIS buffer, and eluted with a TRIS gradient of 0.01−0.5 M. The cytochrome fraction is the first colored band to come out of the column. After concentration in a Diaflo using YM5 membranes, this fraction was loaded onto a HTP column equilibrated with 0.01 M TRIS buffer and eluted using a 0.01−0.3 M phosphate gradient. Cytochrome c_3 elutes at about 0.2 M. The fractions were collected, concentrated using a Diaflo with YM5 membranes, and loaded onto a Superdex 75 column (Pharmacia) equilibrated with 0.1 M NaCl and 0.05 M TRIS buffer. The protein is eluted using the same buffer. The purity of the final fraction was checked by visible spectroscopy, $A_{552red}/A_{280ox} \geq 2.9$. The protein was then dialyzed against deionized water at 4 °C and lyophilized.

NMR Spectroscopy. The protein was lyophilized twice from D_2O (99.9 atom %) and then dissolved in approximately 500 μL D_2O (99.96 atom %) to a concentration of 2−3 mM.

Complete reduction of the cytochrome was achieved by reaction with catalytic amounts of the enzyme hydrogenase from *D. gigas* in the presence of hydrogen. Intermediate oxidation states were obtained by injecting air in the NMR tube through serum caps after flushing out the hydrogen with argon.

The pH of the reduced and partially reduced samples was measured inside an anaerobic glovebox (Mbraun MB 150-GI), with the oxygen level kept below 0.4 ppm, and was adjusted using NaOD and DCl. The values reported are not corrected for the isotope effect. For the experiments at low temperature, an external cooling bath (Haake G with Haake D8) was used to maintain the sample, the electrode, and the calibration buffers at the working temperature.

NMR data were collected in a Bruker AMX 500 spectrometer at 298 and 276.5 K with 200 ms water presaturation. The NOESY experiments were performed with a mixing time of 25 ms, processed using 1024 × 1024 data points with Gaussian apodization (line broadening = −10 Hz, Gaussian broadening = 0.02) in F_2 and shifted sine bell multiplication (cosine) in F_1. The 1D difference NOE experiments were performed with 1024 scans and analyzed after subtraction of a suitable reference spectrum.

Redox Titrations at 298 K. Visible redox titrations of Dgc3 were performed according to the method described in the literature (*27*) using ca. 2 μM protein solutions in 50 mM TRIS−maleate buffer at pH 5.6 and 8.5. To ensure a good equilibrium between the redox centers and the electrode used to measure the solution potential, the following redox mediators were added to the protein solution (*28*), all at ca. 3 μM final concentration: juglone, duroquinone, indigo tetrasulfonate, indigo disulfonate, 2-hydroxy-1,4-naphthoquinone, anthraquinone-2,7-disulfonate, phenosafranine, safranine O, neutral red, cobalt sepulchrate, diquat, and methyl viologen. The redox titrations were performed at room temperature in a quartz cuvette with stirring. The system was kept anaerobic by continuously flushing the cuvette with humidified argon N46 (Air Liquide) previously passed through a copper catalyst to remove any residual oxygen. The protein was fully reduced with sodium dithionite and then oxidized in steps with air. At each step, the redox potential was measured and the visible spectrum was recorded. Solution potentials were measured with a combined Pt/Ag/AgCl electrode (Ingold) previously calibrated using freshly prepared saturated quinhydrone solutions at pH 4.0 and 7.0, and all spectra were recorded with a slit width of 0.5 nm in a Shimadzu UV-260 spectrophotometer.

Because the contribution of the redox mediators to the optical density at the α-peak (λ = 552 nm) is not constant throughout the titration, a correction was made by taking the absorbance at the two isosbestic points of the α-peak (λ = 542 and 560 nm) and subtracting their mean value from the absorbance of the α-peak.

Redox Titrations at 277 K. The low-temperature redox titrations were performed at 277 K inside an anaerobic glovebox, using a double-walled titration vessel mounted in a Radiometer TTA60 titration assembly and Hi-Tech Scientific spectrophotometer unit SU-40. The low temperature increases the time necessary to obtain a stable reading of potential, and inside the glovebox oxygen leaks into the sample are avoided. A combined Pt/Ag/AgCl microelectrode (Microelectrodes Inc.) was used to make the measurements and was calibrated as described above, taking care to correct for the temperature dependence of the reference electrode (*29*). On the basis of the properties published in the literature (*28*), the following mixture of redox mediators was added to the protein solution: methylene blue, indigo tetrasulfonate, indigo trisulfonate, indigo disulfonate, anthraquinone-2,7-disulfonate, anthraquinone-2-sulfonate, safranine O, neutral red, diquat, and methyl viologen. The working temperature was controlled to ±0.5 K using an external cooling bath, and the data were obtained at pH 8.5 in TRIS−maleate 0.1 M buffer. The concentration of both the protein and the mediators was approximately 2 μM. The protein was reduced in steps by small additions of a 2 mM sodium dithionite solution prepared in 10 mM TRIS−maleate buffer at pH 8.5. After each addition, the redox potential was measured and the absorbance change of the cytochrome at the α-peak was measured at a single wavelength. To correct the results for the contribution of the absorbance change of the mediators, titrations were performed in the absence of protein and the results were subtracted to separate the contribution of the cytochrome.

Modeling. The properties of a general system with *n* redox or ionizable centers may be described in terms of the relative populations of 2^n microstates, 32 in the present case (*15*). The energies of the microstates are, in principle, independent but may be expressed as sums of terms for each center and interactions between them. If, as in Dgc3, there is no evidence for major changes in conformation between the microstates, only two-center interactions need be considered. Thus, four redox potentials and one pK_a plus 10 two-center interaction energies (six heme−heme and four redox−Bohr)

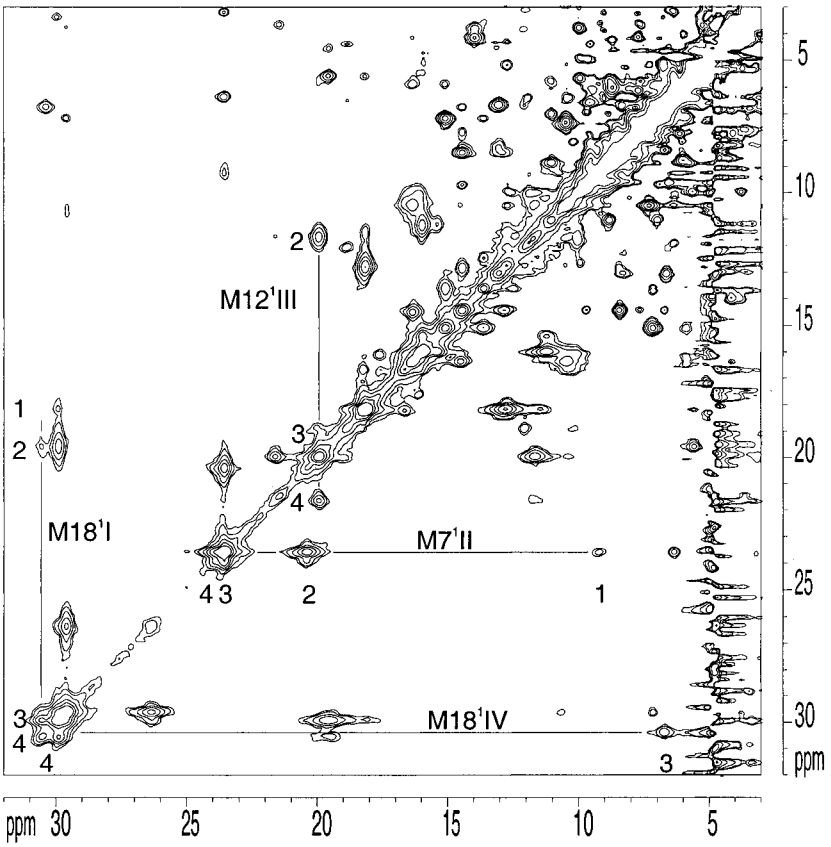

FIGURE 1: NOESY spectrum of Dgc3 obtained at 298 K and pH 5.4. Continuous lines connect exchange signals from the same heme methyl. Other exchange cross-peaks can be observed, under different redox or spectral conditions. The heme methyls followed are identified next to each line using IUPAC−IUB *(30)* recommended nomenclature and roman numbers to identify the respective heme. Arabic numbers in bold indicate the redox stage corresponding to each signal.

are sufficient to characterize the system at any pH or solution potential. The total reduced heme in Dgc3 or the fractional oxidation of any heme at any stage of oxidation is, therefore, a function of 15 energy parameters. These parameters are optimized to fit experimental data using the Marquardt method, assuming that the pH or solution potential is accurately known for each data point.

A computer program (*13*, *15*) was adapted to fit the thermodynamic model of five interacting charged centers simultaneously to the NMR and visible data sets at each temperature. The half-height line widths of the NMR signals were used as a measure of the uncertainty of each chemical shift. The visible data points were assumed to have equal experimental errors (±5 mV) for the titrations at both 298 and 277 K.

RESULTS AND DISCUSSION

When cytochrome c_3 is in fast intramolecular electron exchange and slow intermolecular electron exchange, each heme substituent displays five discrete NMR signals, corresponding to each of the five possible macroscopic population ensembles (stages) connected by four steps of one electron (*12*). At each stage and in the absence of extrinsic paramagnetic effects, the chemical shift of a heme substituent is a function of the oxidized fraction of this particular heme, and only the relative intensity of the signals changes with the redox potential of the solution. The existence of a redox−Bohr effect spatially modulated for each heme results in modifications of the redox potentials, making the oxidized fraction of each heme at each stage pH dependent. Thus, the chemical shift of the signals define macroscopic pK_a values for each oxidation stage (*15*).

Heme methyl resonances provide the most easily identified NMR signals of heme substituents and also display some of the largest paramagnetic shifts, making them ideal to follow throughout the redox titration. Four methyl group resonances (methyls 18^1I, 7^1II, 12^1III, and 18^1IV, with roman numbers indicating the order of heme attachment to the polypeptide chain), each assigned to one of the four hemes (*18*), were followed throughout the NMR redox titration. These methyls point toward the protein surface, and so the extrinsic pseudocontact contributions to their paramagnetic shifts is minimized (*11*). The resonance positions and line widths were measured at each pH and oxidation stage at both temperatures.

A NOESY spectrum of Dgc3 in an intermediate state of oxidation is shown in Figure 1, with the redox exchange pattern of the selected heme methyl resonances indicated.

The chemical shifts of the four methyls at each oxidation stage and at different pH values are reported in Figures 2 and 3 at 298 and 276 K, respectively. The redox titrations followed by visible spectroscopy are shown in Figure 4. The thermodynamic parameters calculated for Dgc3 are presented in Table 1, where the reference state is the fully reduced and protonated protein. The diagonal terms are the energies for oxidation of the hemes and for deprotonation of the ionizable center, whereas the off-diagonal terms are the redox

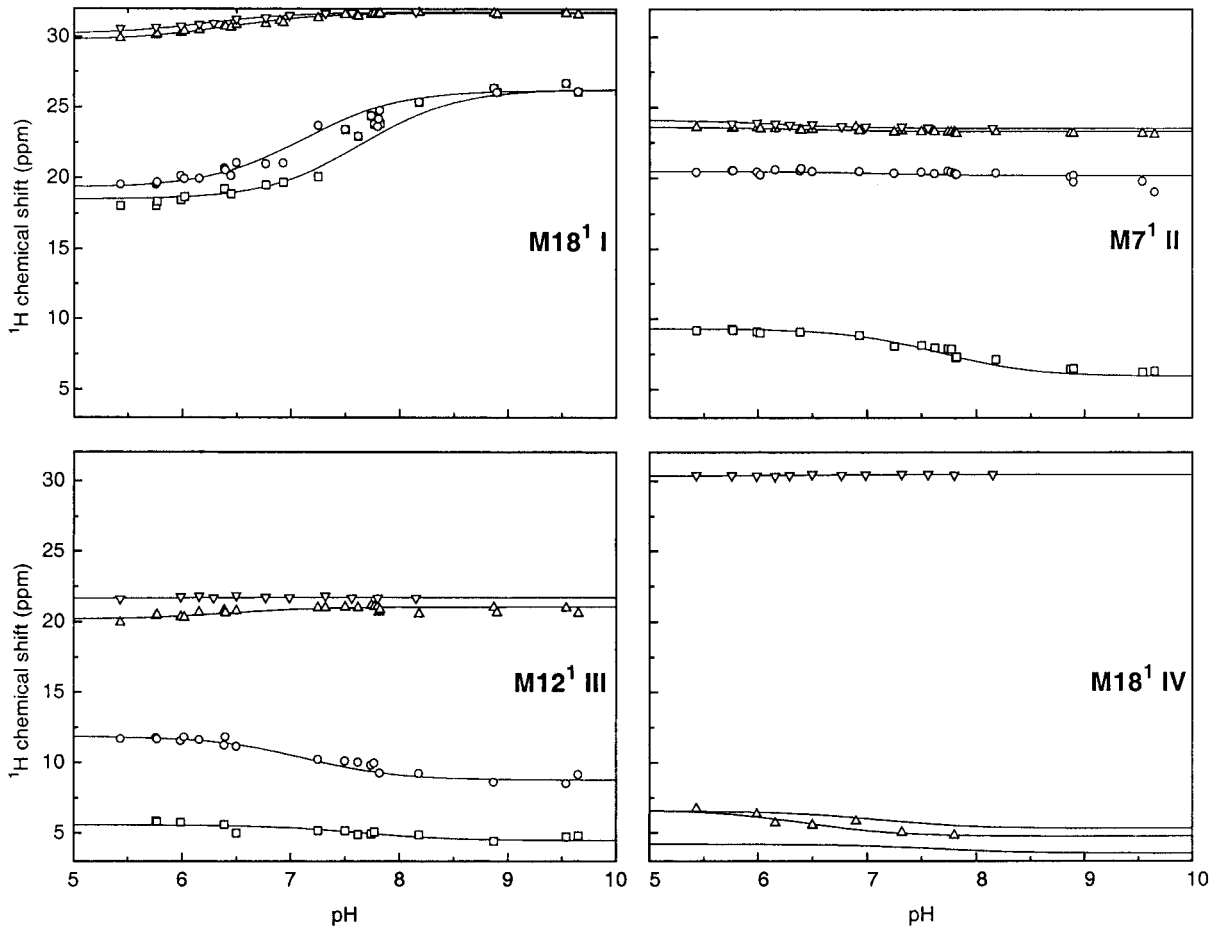

FIGURE 2: Chemical shifts of heme methyl resonances measured at 298 K. Symbols □, ○, △, and ▽ indicate oxidation stages 1, 2, 3, and 4, respectively. IUPAC−IUB nomenclature is used to identify the methyls followed, and the hemes are indicated by roman numbers. The lines were calculated using the thermodynamic data given in Table 1A.

and redox−Bohr interaction energies. The standard errors associated with each parameter are indicated in parentheses.

The results show that the mediators in the redox titrations followed by visible spectroscopy do not participate in specific interactions capable of changing the redox properties of the hemes. Otherwise, a single set of parameters would not fit both the visible and NMR data obtained at the same temperature.

The small oxidized fraction of heme IV in stages 1 and 2 leaves the corresponding signals buried in the crowded diamagnetic region, and as a consequence, no signals were observed. This results in a slight increase in the uncertainty associated with the parameters obtained for heme IV, as can be seen from some of their standard errors. In particular, there is a significant negative correlation between the heme I−heme IV interaction energy and the microscopic redox potential of heme IV. However, removing the interaction between heme I and heme IV results in a worse fit at both temperatures.

The visible data obtained at a single wavelength at 277 K could not be fitted satisfactorily with the assumption that all the hemes have equal extinction coefficients. Simultaneous fits of the visible and NMR data with increasing weight for the visible data leads to a considerable degradation of the quality of the fit of the NMR data without any significant improvement of the fit to the visible. However, the data can be fitted by assuming that the highest potential heme accounts for 30% of the total absorbance change. This modification is supported by the report that this heme is spectroscopically distinct from the others (*31*). Because the measurements were made at a single wavelength, it was not possible to follow the maximum of the α-band as it changed its position along the redox titration, and so these small deviations in the position of the maximum result in changes of the measured absorbance. The calcium ion observed close to heme IV in the crystal structure of Dgc3 (*5*) is unlikely to be responsible for this spectroscopic difference because similar differences have been observed for other cytochromes c_3 (*31*−*33*). A more plausible candidate is the electrostatic environment around heme IV, which is very rich in lysine residues in most cytochromes c_3.

Table 1 shows that the largest redox−Bohr effect involves heme I, a similar result to that obtained for Dvc3 (*13*−*15*, *21*). It remains to be determined whether the effect in Dgc3 is also mediated by the propionates of this heme, but the present results indicate that this is likely to be the case because the magnitude of the redox−Bohr interaction with heme I is similar for both proteins at room temperature. Furthermore, as in Dvc3, the weakest interaction is with heme IV.

Table 1 also shows a strong positive redox cooperativity between hemes II and III. Pure electrostatic interactions between the hemes contribute negatively to their cooperativity, and so a conformational modification, which may be highly localized, is required to explain the interaction between these two hemes (*13*, *15*, *25*). Although Dvc3

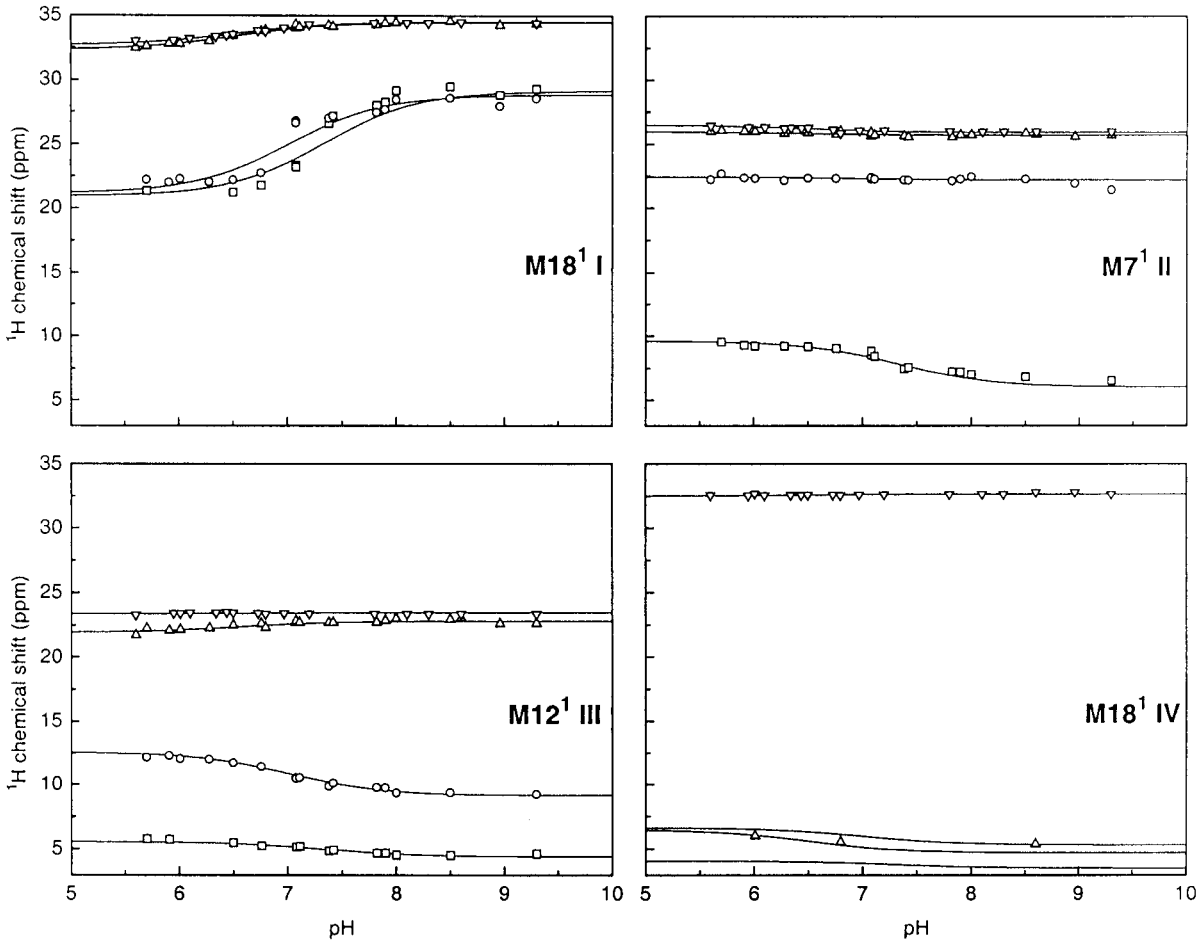

FIGURE 3: Chemical shifts of heme methyl resonances measured at 276.5 K. Symbols □, ○, △, and ▽ indicate stages 1, 2, 3, and 4, respectively. IUPAC−IUB nomenclature is used to identify the methyls followed, and the hemes are indicated by roman numbers. The lines are calculated from the thermodynamic data given in Table 1B.

displays a similar positive cooperativity between the second and third to be oxidized, it involves a different pair of hemes (I and II). This observation supports the proposal that the two central hemes in terms of order of redox potentials are those which are functionally important, whereas those with higher and lower redox potentials prepare the protein for a two-electron step by means of redox interactions (*34*, *22*). However, this picture is not so clear-cut for Dgc3 because three hemes (I, II, and III) have very similar redox potentials close to pH 7, which enable the uptake or release of up to 3 electrons in Dgc3 within a very narrow range of redox potentials, as shown in Figure 5.

Figure 6 shows the pH dependence of the macroscopic redox steps in Dgc3. In Dvc3, the second and third macroscopic redox steps cross over at physiological pH. This does not occur in Dgc3 because the two dominant hemes in these steps, hemes II and III, have very similar redox−Bohr interactions. Thus, the change in the protonation state of the protein provides only a small assistance to the cooperativity, as shown by the smaller separation in the curves close to pH 7.

Current theoretical models predict that the values for the midpoint redox potentials result from contributions of different origins (*35*−*38*). From the temperature dependence of the data obtained for Dgc3, the entropic contribution for each parameter can be estimated. Because the data set obtained represents a bare minimum for this purpose, the uncertainty only allows a qualitative discussion. The enthalpic contributions to the redox free energies are not listed because the extrapolation from two data points to 0 K is too uncertain. Table 2 shows that the entropic contribution to the redox potentials is similar for all hemes, in agreement with data obtained for class I *c*-type cytochromes (*39*). Thus, the observation that the entropic term is related to the change in the charge of the center, made for mediator redox couples, may also apply to the hemes in cytochromes (*40*). Because the redox potentials of the hemes are different, the modulation of their redox potentials has to be provided by the influence of the environment around each of the hemes (*41*−*43*). Our data shows that this influence is concentrated in the enthalpic contribution to the free energy, as previously reported for class I cytochromes *c* (*39*).

Bertrand et al. (*44*) obtained different results when studying cytochromes c_3 from *D. vulgaris* Miyazaki F and *D. desulfuricans* (Norway), showing large variations in the values of $T\Delta S^{\circ\prime}$ and $\Delta H^{\circ\prime}$ for the different hemes. However, the data used for that work provided no experimental information on the microscopic redox potentials of the hemes, which therefore had to be estimated with the key assumption that the interaction potentials are temperature independent. The experimental results reported in Table 1 show that this assumption is not valid for Dgc3.

The large and negative entropic change upon deprotonation of the ionizable center is evidence of an increase in ordering

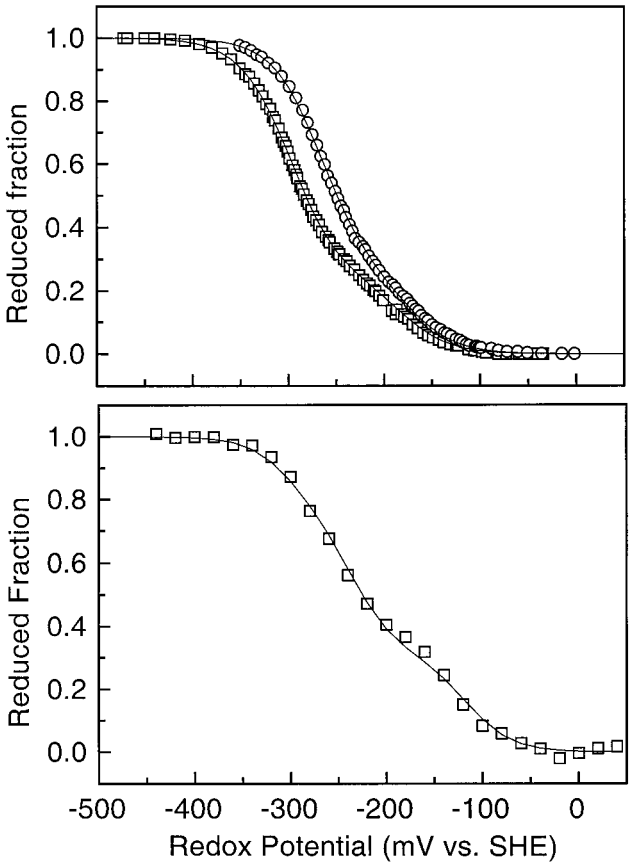

FIGURE 4: Visible redox titration of Dgc3. Top: titrations performed at 298 K. Data points □ and ○ were obtained at pH 8.5 and 5.6, respectively. Bottom: titration performed at 277 K at pH 7.0. The continuous lines were calculated using the thermodynamic data given in Tables 1A and 1B.

Table 1: Thermodynamic Parameters Determined for Dgc3 (in meV)[a]

(A) Parameters Determined at 298 K

center	I	II	III	IV	ionizable
I	**−277(2)**	0(2)	25(2)	−24(6)	−62(2)
II		**−260(2)**	−40(2)	35(3)	−33(2)
III			**−236(2)**	17(2)	−33(2)
IV				**−202(6)**	−10(2)
ionizable					**505(4)**

(B) Parameters Determined at 276.5 K

center	I	II	III	IV	ionizable
I	**−257(4)**	14(3)	34(3)	−11(9)	−46(3)
II		**−239(4)**	−26(3)	44(4)	−20(3)
III			**−215(4)**	28(3)	−19(3)
IV				**−179(9)**	1(3)
ionizable					**441(8)**

[a] Diagonal terms (in bold) are energies of oxidation of the hemes and energy of deprotonation of the ionizable center for the fully reduced and protonated protein. Off-diagonal terms are interaction energies between the centers. Standard errors are given in parentheses.

through electrostatic interactions, as expected for the ionization of uncharged groups such as heme propionates. The entropic contributions to the redox interaction energies, listed in Table 2, are broadly similar, and there is no clear distinction between those which contribute to positive or negative cooperativities. Positive redox cooperativities emerge at temperatures high enough for $T\Delta S^{\circ\prime}$ to outweigh the value of $\Delta H^{\circ\prime}$, and for some cases, $\Delta H^{\circ\prime}$ is small enough

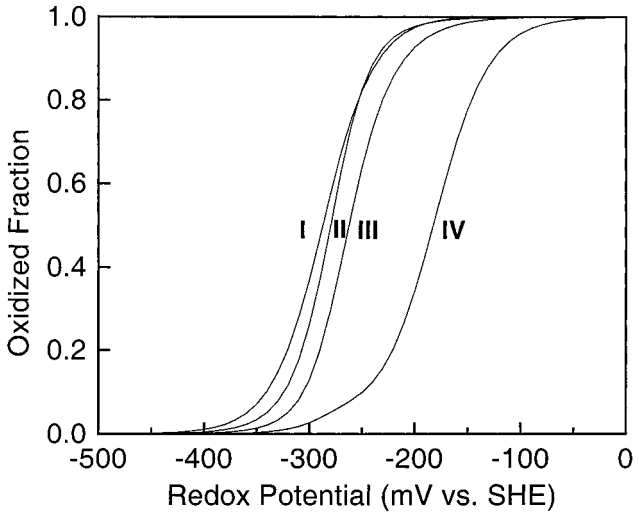

FIGURE 5: Reduced fraction of each heme versus the redox potential calculated for pH 7.0 at 298 K using the parameters listed in Table 1. The hemes are indicated by roman numbers next to each line.

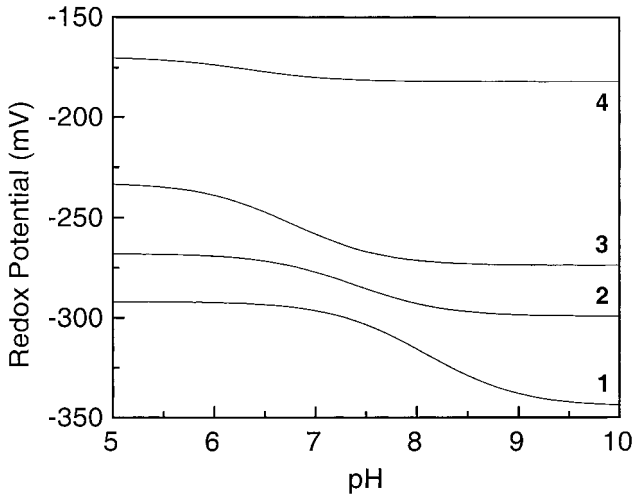

FIGURE 6: pH dependence of the macroscopic redox potentials determined for Dgc3 at 298 K, calculated from the parameters listed in Table 1. Numbers near the lines indicate the macroscopic redox step.

Table 2: Entropic Contribution ($\Delta S^{\circ\prime}$ in J K^{-1} mol^{-1}) to the Variations in the Free Energies Reported in Table 1

center	I	II	III	IV	ionizable
I	92	65	44	57	68
II		100	66	42	58
III			96	50	64
IV				105	52
ionizable					−285

for this to occur even at 277 K. In these cases the dominance of the entropic contribution is understandable because the positive interactions are indicative of a conformational change.

The macroscopic pK_as for the various redox stages, which are a function of the redox and redox−Bohr interactions, are necessarily temperature dependent and are reported in Table 3.

CONCLUSIONS

The information obtained on the temperature dependence of the microscopic thermodynamic parameters is fundamental

Table 3: Macroscopic pK_as of the Ionizable Center of Dgc3 at Different Stages of Oxidation

	stage				
K	0	1	2	3	4
276.5	8.04	7.34	7.01	6.52	6.52
298.0	8.54	7.65	7.12	6.42	6.21

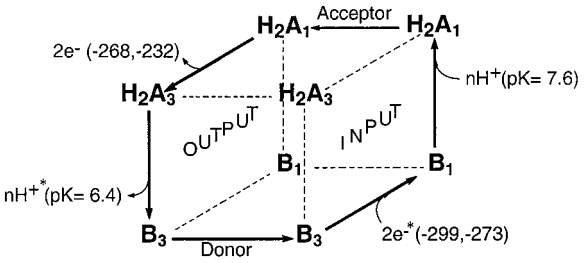

FIGURE 7: The cubane diagram for energy transduction applied to Dgc3. The functional pathway is drawn with arrows cycling between oxidation stages 1 (molecule with one heme oxidized) and 3 (three hemes oxidized). Hydrogenase supplies protons and electrons to the cytochrome which, upon diffusion to the acceptor, transfers the electrons. Due to the lowering of the pK_a, the protons can be released and the cytochrome is ready to resume the cycle. The input and output faces of the cube indicate the states where the electrons and protons are taken up (coupled to hydrogenase) and released (coupled to the transmembrane electron and proton carriers). High-energy protons and electrons are indicated with an asterisk.

for understanding the factors controlling the redox potentials in these complex systems and may be incorporated into refined electrostatic models for these proteins (*45*, *46*). The entropic contribution to the total free energy change is evaluated in this work. The observation that the redox potentials of the hemes are modulated by changes in the enthalpic contribution to the reaction free energy is of particular interest and is in agreement with the interpretation of electrostatic calculations performed for the tetraheme cytochrome of the photosynthetic reaction center from *Rhodopseudomonas viridis* (*36*).

The differences observed between Dgc3 and Dvc3, both in the order of the redox potentials of the hemes and in the sign of the redox cooperativities, indicate that the relation between the structure of the core and the function of the protein is not simple. The architecture of the heme core appears to be designed to allow the cytochrome to take up more than one electron in a narrow range of potentials. This is accomplished by a network of functional interactions which involves positive redox cooperativities between two of the hemes, not necessarily the same pair in different proteins, and redox−Bohr cooperativities between the hemes and an ionizable center. In both cases studied, the redox−Bohr effect is strongest with heme I, and the data reported in this article provides evidence that the charged groups involved are the propionates of heme I in Dgc3, as in Dvc3. The structural basis for the redox−Bohr effect was attributed to the heme propionates for several cytochromes (*14*, *15*, *47*).

The thermodynamic properties warrant the interpretation of the results with respect to a "cubane" scheme describing the energy transduction process (Figure 7), as previously done for Dvc3. Low potential electrons (high energy) and high pK_a protons are received from the hydrogenase and subsequently released as higher potential electrons (lower energy) and lower pK_a protons. Discrete input and output states can be defined for both protons and electrons, ensuring that effective gating of these states also operates in Dgc3 (*48*). This is a fundamental requirement for energy transduction, which has been defined as specificity of the first kind (*49*). For the case of Dgc3, in addition to the thermodynamic data, kinetic data is available for its reduction with sodium dithionite (*50*). Heme IV is the fastest heme to be reduced or oxidized, and computer models of complexes of cytochrome c_3 with physiological and nonphysiological redox partners (*51*, *52*) show that this is also the heme which interacts more closely with the redox partners, making it the putative gate for electron transfer. The individual reduction rate constants of the individual hemes show that the largest difference between the protonated and deprotonated forms of the protein is observed for heme I, with more rapid reduction in the protonated form. This heme has the second fastest reduction rate but has the lowest redox potential. Thus, since the intramolecular electron exchange is fast, it drains the electrons received to hemes II and III. Furthermore, the difference in the reduction rates between the protonated and deprotonated forms favors the switching to the protonated form of the protein upon reduction, establishing proper step control. The observed difference of the electron-transfer rates is in agreement with the proposed functional specificity of the second kind, providing kinetic control of the transitions so that the pathway required for energy transduction is favored over others which would result in a futile cycle (*49*). The data for Dgc3 fit the proposal made for transmembrane proton pumps that "there may be components of both 'thermodynamic' and 'kinetic' linkage to maximize kinetic versatility and energetic efficiency of the pump" (*49*). The present work broadens the scope of phenomenological similarity between "proton thrusting" (*2*) performed by these soluble systems tetraheme cytochromes c_3 and transmembrane "proton pumping".

REFERENCES

1. Yagi, T., Honya, M., and Tamiya, N. (1968) *Biochim. Biophys. Acta 153*, 699−705.
2. Louro, R. O., Catarino, T., LeGall, J., and Xavier, A. V. (1997) *J. Biol. Inorg. Chem. 2*, 488−491.
3. Higuchi, Y., Kusunoki, M., Matsuura, Y., Yasuoka, N., and Kakudo, M. (1984) *J. Biol. Chem. 172*, 109−139.
4. Matias, P. M., Frazão, C., Morais, J., Coll, M., and Carrondo, M. A. (1993) *J. Mol. Biol. 234*, 680−699.
5. Matias, P. M., Morais, J., Coelho, R., Carrondo, M. A., Wilson, K., Dauter, Z., and Sieker, L. (1996) *Protein Sci. 5*, 1342−1354.
6. Czjzek, M., Payan, F., Guerlesquin, F., Bruschi, M., and Haser, R. (1994) *J. Mol Biol. 243*, 653−667.
7. Morais, J., Palma, P. N., Frazão, C., Caldeira, J., LeGall, J., Moura, I., Moura, J. J. G., and Carrondo, M. A. (1995) *Biochemistry 34*, 12830−12841.
8. Messias, A. C., Kastrau, D. H. W., Costa, H. S., LeGall, J., Turner, D. L., Santos, H., and Xavier, A. V. (1998) *J. Mol. Biol. 281*, 719−739.
9. Coutinho, I. B., Turner, D. L., LeGall, J., and Xavier, A. V. (1992) *Eur. J. Biochem. 209*, 329−333.
10. Turner, D. L., Salgueiro, C. A., Schenkels, P., LeGall, J., and Xavier, A. V. (1995) *Biochim. Biophys. Acta 1246*, 24−28.
11. Salgueiro, C. A., Turner, D. L., and Xavier, A. V. (1997) *Eur. J. Biochem. 244*, 721−734.
12. Santos, H., Moura, J. J. G., Moura, I., LeGall, J., and Xavier, A. V. (1984) *Eur. J. Biochem. 141*, 283−296.

13. Turner, D. L., Salgueiro, C. A., Catarino, T., LeGall, J., and Xavier, A. V. (1994) *Biochim. Biophys. Acta 1187*, 232−235.
14. Park, J.-S., Ohmura, T., Kano, K., Sagara, T., Niki, K., Kyogoku, Y., and Akutsu, H. (1996) *Biochim. Biophys. Acta 1293*, 45−54.
15. Turner, D. L., Salgueiro, C. A., Catarino, T., LeGall, J., and Xavier, A. V. (1996) *Eur. J. Biochem. 241*, 232−235.
16. Turner, D. L., Salgueiro, C. A., LeGall, J., and Xavier, A. V. (1992) *Eur. J. Biochem. 210*, 931−936.
17. Coutinho, I. B., Turner, D. L., LeGall, J., and Xavier, A. V.-(1993) *Biochem. J. 294*, 899−908.
18. Piçarra-Pereira, M. A., Turner, D. L., LeGall, J., and Xavier, A. V. (1993) *Biochem. J. 294*, 909−915.
19. Louro, R. O., Pacheco, I. P., Turner, D. L., LeGall, J., and Xavier, A. V. (1996) *FEBS Lett. 390*, 59−62.
20. Salgueiro, C. A., Turner, D. L., Santos, H., LeGall, J., and Xavier, A. V. (1992) *FEBS Lett. 314*, 155−158.
21. Salgueiro, C. A., Turner, D. L., LeGall, J., and Xavier, A. V. (1997) *J. Biol. Inorg. Chem. 2*, 343−349.
22. Louro, R. O., Catarino, T., Salgueiro, C. A., LeGall, J., and Xavier, A. V. (1996) *J. Biol. Inorg. Chem. 1*, 34−38.
23. Odom, J. M., and Peck, H. D., Jr. (1981) *FEMS Microbiol. Lett. 12*, 47−50.
24. Saraiva, L. M., Salgueiro, C. A., da Costa, P. M., Messias, A. C., LeGall, J., van Dongen, W. M. A. M., and Xavier, A. V. (1998) *Biochemistry 37*, 12160−12165.
25. Coletta, M., Catarino, T., LeGall, J., and Xavier, A. V. (1991) *Eur. J. Biochem. 202*, 1101−1106.
26. LeGall, J., Mazza, G., and Dragoni, N. (1965) *Biochim. Biophys. Acta 99*, 385−387.
27. Dutton, P. L. (1978) *Methods Enzymol. 54*, 411−435.
28. Clark, W. M. (1972) *Oxidation−Reduction Potentials of Organic Systems*, Robert E. Krieger Publishing Co., Huntington, NY.
29. Bühler, H., and Galster, H. (1980) *Ingold booklets (E-Th2)* Ingold, Zürich.
30. IUPAC−IUB Joint Commission on Biochemical Nomenclature (1988) *Eur. J. Biochem. 178*, 277−328.
31. Schlereth, D. D., Fernández, V. M., and Mäntele, W. (1993) *Biochemistry 32*, 9199−9208.
32. Kazanskaya, I., Lexa, D., Bruschi, M., and Chottard, G. (1996) *Biochemistry 35*, 13411−13418.
33. Yagi, T. (1984) *Biochim Biophys. Acta 767*, 288−294.
34. Xavier, A. V. (1986) *J. Inorg. Biochem. 28*, 239−243.
35. Moore, G. R., Pettigrew, G. H., and Rogers, N. K. (1986) *Proc. Natl. Acad. Sci. U.S.A. 83*, 4998−4999.
36. Gunner, M. R., and Honig, B. (1991) *Proc. Natl. Acad. Sci. U.S.A. 88*, 9151−9155.
37. Langen, R., Brayer, G. D., Berghuis, A. M., McLendon, G., Sherman, F., and Warshel, A. (1992) *J. Mol. Biol. 224*, 589−600.
38. Jensen, G. H., Warshel, A., and Stephens, P. J. (1994) *Biochemistry 33*, 10911−10924.
39. Battistuzzi, G., Borsari, M., Sola, M., and Francia, F. (1997) *Biochemistry 36*, 16247−16258.
40. Liu, Y., Seefeldt, L. C., and Parker, V. D. (1997) *Anal. Biochem. 250*, 196−202.
41. Churg, A. K., and Warshel, A. (1986) *Biochemistry 25*, 1675−1681.
42. Gunner, M. R., Alexov, E., Torres, E., and Lipovaca, S. (1997) *J. Biol. Inorg. Chem. 2*, 126−134.
43. Warshel, A., Papazyan, A., and Muegge, I. (1997) *J. Biol. Inorg. Chem. 2*, 143−152.
44. Bertrand, P., Mbarki, O., Asso, M., Blanchard, L., Guerlesquin, F., and Tegoni, M. (1995) *Biochemistry 343*, 11071−11079.
45. Soares, C. M., Martel, P. J., and Carrondo, M. A. (1997) *J. Biol. Inorg. Chem. 2*, 714−727.
46. Soares, C. M., Martel, P. J, Mendes, J., and Carrondo, M. A. (1998) *Biophys. J. 74*, 1708−1721.
47. Moore, G. R., Pettigrew, G. W. (1990) in *Cytochromes c, evolutionary structural and physicochemical aspects*, pp 348−361, Springer-Verlag, London.
48. Blair, D. F., Gelles, J., and Chan, S. I. (1986) *Biophys. J. 50*, 713−733.
49. Krab, K., and Wikstrom, M. (1987) *Biochim. Biophys. Acta 895*, 25−39.
50. Catarino, T., Coletta, M., LeGall, J., and Xavier, A. V. (1991) *Eur. J. Biochem. 202*, 1107−1113.
51. Stewart, D. E., LeGall, J., Moura, I., Moura, J. J. G., Peck, H. D., Jr., Xavier, A. V., Weiner, P. K., and Wampler, J. E. (1988) *Biochemistry 27*, 2444−2450.
52. Palma, P. N., Moura, I., LeGall, J., Van Beeumen, J., Wampler, J. E., and Moura, J. J. G. (1994) *Biochemistry 33*, 6394−6407.

BI981505T